

The Free Energy of Small Solute Permeation through the *Escherichia coli* Outer Membrane Has a Distinctly Asymmetric Profile

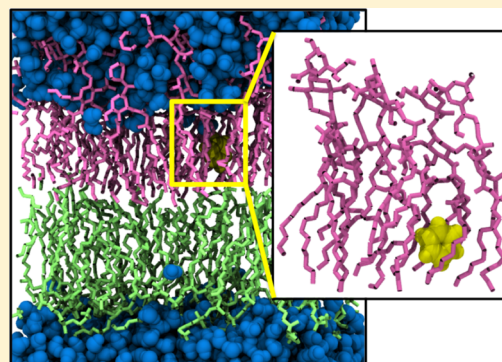
Timothy S. Carpenter,[†] Jamie Parkin,[‡] and Syma Khalid^{*,‡}

[†]Lawrence Livermore National Laboratory, Livermore, California 94550, United States

[‡]School of Chemistry, University of Southampton, Southampton, U.K. SO17 1BJ

Supporting Information

ABSTRACT: Permeation of small molecules across cell membranes is a ubiquitous process in biology and is dependent on the principles of physical chemistry at the molecular level. Here we use atomistic molecular dynamics simulations to calculate the free energy of permeation of a range of small molecules through a model of the outer membrane of *Escherichia coli*, an archetypical Gram-negative bacterium. The model membrane contains lipopolysaccharide (LPS) molecules in the outer leaflet and phospholipids in the inner leaflet. Our results show that the energetic barriers to permeation through the two leaflets of the membrane are distinctly asymmetric; the LPS headgroups provide a less energetically favorable environment for organic compounds than do phospholipids. In summary, we provide the first reported estimates of the relative free energies associated with the different chemical environments experienced by solutes as they attempt to cross the outer membrane of a Gram-negative bacterium. These results provide key insights for the development of novel antibiotics that target these bacteria.



The membranes that surround bacteria provide the cells with a sophisticated layer of protection. Understanding the molecular processes by which solutes permeate across bacterial cell membranes is an important point to consider when developing novel antibacterial agents. Interaction with cell membranes will occur whether the antibiotics are designed to destroy the bacterial cell through disruption of the membrane or interfere with some cellular process that takes place within the cell; in the latter case, permeation of the membrane is necessary to gain access to the interior of the cell. Many pathogenic bacteria are Gram-negative; thus, their cell envelopes are composed of two membranes. The outer membrane (OM) is asymmetric in nature. The outer leaflet is composed of lipopolysaccharide (LPS) molecules, whereas the inner leaflet contains a mixture of Zwitterionic and anionic phospholipids. Previously it has been shown that the components of the outer leaflet diffuse an order of magnitude slower than the phospholipids of the inner leaflet; this is thought to be a consequence of the tightly packed head groups, which are cross-linked by divalent cations, and the greater number of hydrophobic tails per lipid of lipopolysaccharide compared to phospholipids.¹ The arrangement of the two leaflets is one of the molecular origins of the characteristic impermeability of the outer membrane.² While permeation of small molecules across most cell membranes commonly occurs through passive diffusion, permeation across the OM of Gram-negative bacteria is usually thought to require assistance either from proteins or degradation of the integrity of the membrane, for example for the latter, through disruption of the cation-

cross-linked headgroups of LPS. The design of novel antibiotics must therefore consider how these molecules will negotiate the outer membrane. In particular, identifying the location of the energetic barriers that render permeation difficult would enable rational modification of drugs to ease their passage across the OM. Computational approaches such as umbrella sampling, which is a particular implementation of molecular dynamics, provide a route to estimate free energy of permeation.^{3,4} However, the chemical complexity of biological membranes can present somewhat of an obstacle to achieving well-sampled trajectories. We have employed atomistic molecular dynamics simulations using the umbrella sampling technique with the weighted histogram analysis method (WHAM)⁵ to construct the potential of mean force (PMF) curves for the permeation of ethane, hexane, benzene, acetic acid, and ethanol through a model of the *Escherichia coli* OM containing 16 ReLPS molecules in the outer leaflet and 2 cardiolipin, 18 phosphatidylethanolamine, and 2 phosphatidylglycerol molecules in the inner leaflet. Each PMF curve is constructed from at least 100 umbrella sampling windows, where each window is simulated for ~200 ns.

The PMF profiles are distinctly asymmetric (Figure 1). All three hydrophobic solutes—hexane, ethane, and benzene—have similar profiles overall; the PMF is essentially flat in the bulk water region on the phospholipid side. $G(z)$ does not

Received: June 24, 2016

Accepted: August 12, 2016

Published: August 12, 2016

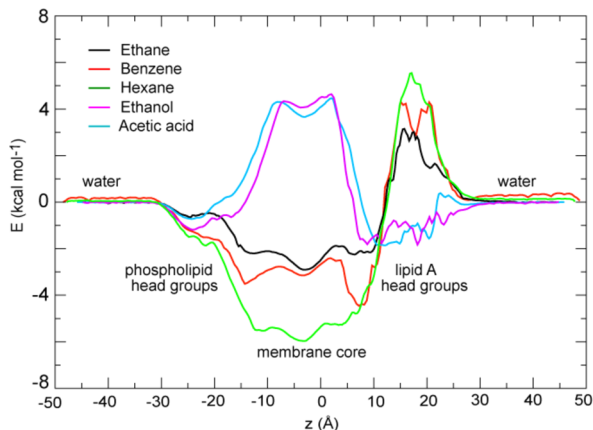


Figure 1. Potential of mean force curves for the five solutes: ethane, benzene, hexane, ethanol, and acetic acid.

change appreciably upon entering the phospholipid headgroup region. It decreases when moving deeper along the hydrocarbon tails and then rises when entering the highly charged LPS headgroup region. Finally, the curve flattens again at the bulk water region on the LPS side of the bilayer. The energetic barrier at the LPS headgroup region (corresponding to $z \sim 13\text{--}25\text{ \AA}$) is most pronounced for hexane, which is likely a consequence of the longer hydrophobic length of hexane compared to benzene and ethane. The maximum free energy in the LPS headgroup regions from our simulations is $\sim 6\text{ kcal/mol}$ for hexane, $< 5\text{ kcal/mol}$ for benzene, and $\sim 3\text{ kcal/mol}$ for ethane.

The slow diffusing LPS molecules have headgroups tightly cross-linked by divalent cations and thus “trap” the hydrophobic solutes in unfavorable water-filled cavities between a number of polar and charged moieties. The large LPS headgroups have enough flexibility to “bend away” from hydrophobic solutes on the time scales of our simulations. Comparison of the minimum LPS–hexane and LPS–benzene distances reveals that in general benzene occupies a position ~ 2

\AA closer to the LPS headgroups than hexane in equivalent umbrella sampling windows in the headgroup region, indicating that the LPS molecules are repelled further away from hexane (Figure 2). This is also further highlighted when the numbers of solute–LPS contacts (where contact is defined as a distance of $\leq 6\text{ \AA}$) are compared for benzene and hexane in the LPS headgroup region (data shown in the Supporting Information). There are ~ 3 times more LPS–benzene contacts than LPS–hexane contacts, despite the molecules being similar in size. The number of contacts for ethane is much lower than that for both benzene and hexane because of its smaller size.

Our observations show that the LPS headgroups move away from the hexane as would be expected because of their anionic nature. Given their large size and slow rate of diffusion, they remain positioned away from hexane. Water is smaller, faster moving, and polar rather than formally charged; the combined effect of these properties is that water is able to move in and out of the interstitial voids in the headgroup area. Figure 3 shows some representative center-of-mass plots of hexane, water, and LPS phosphates groups, which demonstrate their relative mobilities in the headgroup region.

Previously reported MD simulation studies of small solute permeation through symmetrical phospholipid bilayers have revealed small aliphatic chains such as propane have similar barriers through the headgroup region of PC and PE lipid headgroups as benzene.^{3,4,6} Intriguingly, we do not observe any appreciable barriers to entry of any of the solutes into the head groups of the phospholipid leaflet. Visual inspection of the umbrella sampling window corresponding to these regions reveals that this is due to the high mobility of the phospholipids, which are able to rearrange locally, such that the hydrophobic solutes become exposed to parts of the lipid tail regions. We note that our simulations for each umbrella window are substantially longer in length than those reported in similar studies of solute permeation across lipid bilayers; therefore, we likely observe lipid rearrangement that is not possible in shorter simulations.^{3,4} We have plotted time-dependent radial distribution functions for benzene and hexane

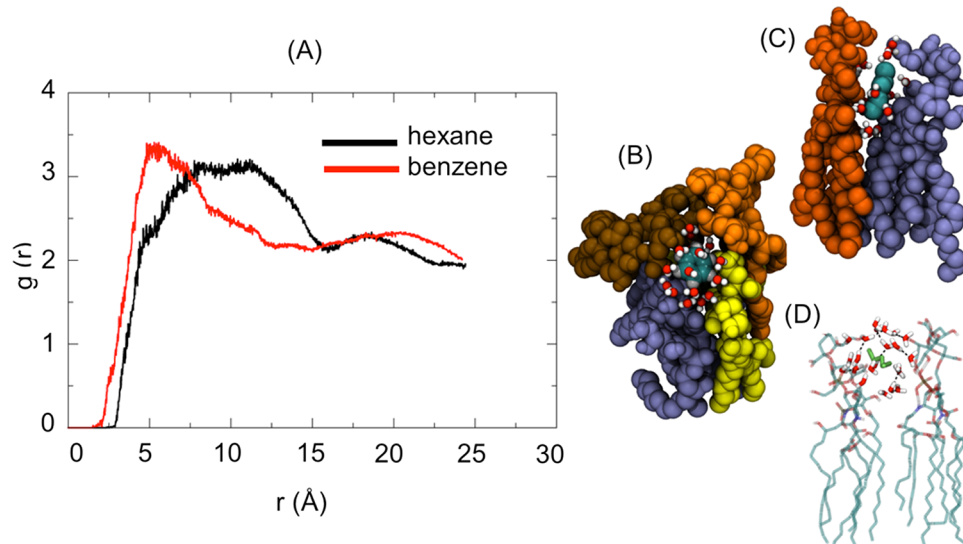


Figure 2. (A) Radial distribution function of LPS molecules around benzene and hexane. (B) Space-filling diagram of benzene located within a pocket formed by four LPS molecules, with water molecules covering the pocket. (C) Space-filling representation of hexane with only two LPS residues that are within 0.6 nm . Water molecules are located above and below hexane. (D) Stick representation showing the same effect as in panel C from a different simulation snapshot.

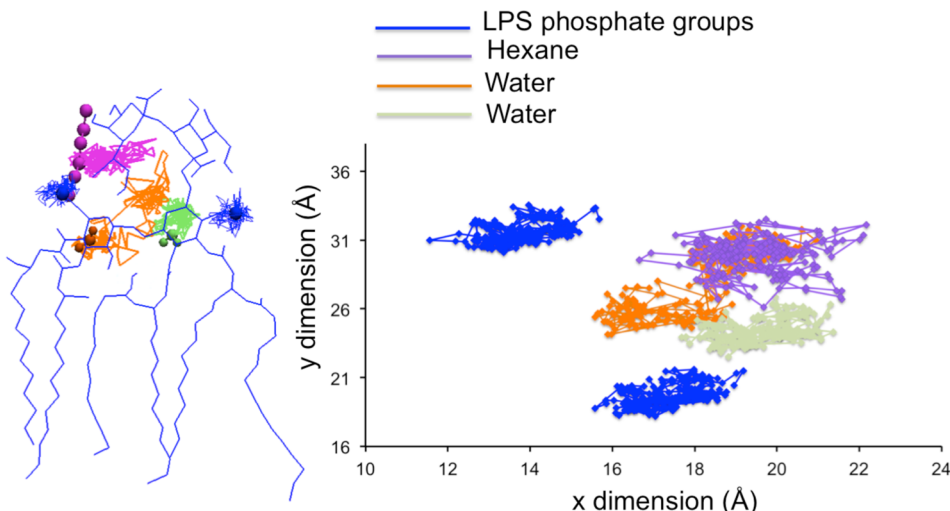


Figure 3. Representative center of mass trajectories of hexane (purple), water (orange and green), and LPS phosphate groups (blue) over the last 20 ns (out of a total of 200 ns) of a simulation in which hexane is in the LPS headgroup area. The LPS phosphates are not as mobile as the other molecules. In particular, the water molecule represented by the orange line is able to move substantially more than the LPS phosphate groups.

with the phosphorus atoms of the phospholipids (*Supporting Information*); these data clearly show that the lipids are rearranging around the solutes up to \sim 100 ns of simulation. Furthermore, we note that Chetwynd et al. also did not observe any appreciable barrier to entry of a hydrophobic transmembrane peptide into the headgroup region of a phospholipid bilayer from time scale simulations per umbrella sampling window similar to those reported here.⁷ These local rearrangements are not observed with LPS because of a combination of factors: their headgroups are tightly cross-linked by divalent cations; the molecules diffuse an order of magnitude slower than phospholipids; and the charged region of LPS molecules is substantially larger than phospholipids.

Favorable hydrophobic interactions with the lipid tails in the core of the membrane provide an energetic well for the hydrophobic solutes in this region. The minimum value of ΔG for each of the hydrophobic solutes within the core of the membrane and corresponding data from experimental studies of solute transfer from water to hexadecane are given in Table 1. The appropriate experimental data for comparison with asymmetric bilayers containing LPS and phospholipids is not available in the literature for direct comparison. The most favorable free energy in the core is for hexane with the

minimum corresponding to -5.8 kcal/mol; this makes sense given it is the most hydrophobic of the three solvents.

The PMF curve for benzene is particularly interesting, because while the other solutes have generally symmetric curves in areas other than the headgroup regions, benzene shows a distinct asymmetry in the tail regions too, with more favorable energetics corresponding to the lipid A tails of LPS compared to the phospholipid tails. The difference in free energy between the two regions may be partially explained by the greater number of close contacts formed by benzene in the LPS headgroup-tail interface compared to the equivalent region in the phospholipid leaflet; there are \sim 100 more contacts (i.e., instances of interatomic distances between the two molecules being >6 Å) in LPS (Figure 4). Comparison of the equivalent values for hexane shows that there is no overall difference in the number of contacts in the headgroup-tail interface regions of the two leaflets, which corresponds to the symmetrical PMF curve shown in Figure 1.

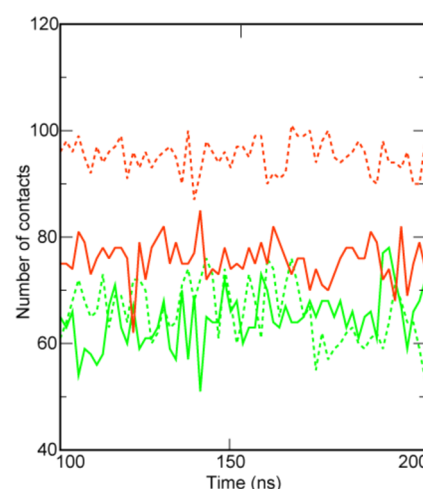


Table 1. Comparison of the Free Energy of Transfer between Water and Hexadecane, ΔG_{exp} , with the Free Energies of Transfer between Water and the Model Bacterial Membrane Used in This Study, ΔG_M

solute	$\ln k^a$	T (K)	ΔG_{exp}^b (kcal/mol)	ΔG_M^c (kcal/mol)
ethane	1.83	298	-1.08^d	-2.7 ± 0.1^d
hexane	4.49	298	-2.66^d	-5.8 ± 0.3^d
benzene	2.15	298	-1.27^d	-3.0 ± 0.2^d
ethanol	-2.19	298	1.30^e	3.8 ± 0.2^e
acetic acid	-3.16	298	1.87^e	3.8 ± 0.3^e

^aThe values of $\ln k$ were obtained from Abraham et al.⁸ ^bThe ΔG_{exp} were calculated using the relationship $\Delta G = -RT \ln K$, where R is the ideal gas constant and T is the temperature. ^c ΔG_M values were recorded as the minima and maxima in the membrane core region for each respective substrate from our simulations. ^dMinimum. ^eMaximum.

Figure 4. Number of contacts between benzene (red) and hexane (green) within the two lipid headgroup-tail interface regions. The dashed lines represent the LPS interface and the solid lines represent the interface of the phospholipids.

The polar solutes, ethanol and acetic acid, do not experience an energetic barrier to entry into the phospholipid or LPS headgroup region. Indeed, as expected they show the opposite general trends compared to the hydrophobic molecules. Within both headgroup regions, hydrogen-bonding interactions stabilize the solutes. The LPS head groups provide a wider region in which there is an energetic well compared to the phospholipids. This is due to the larger size of the LPS head groups which means there is availability of stabilizing hydrogen-bonding moieties over a wider area, with additional hydrogen-bonding capabilities provided by water molecules that penetrate within the head groups; this is highlighted in Figure 5. This region is narrower for the phospholipids, only $\sim 7 \text{ \AA}$ compared to $\sim 16 \text{ \AA}$ for LPS.

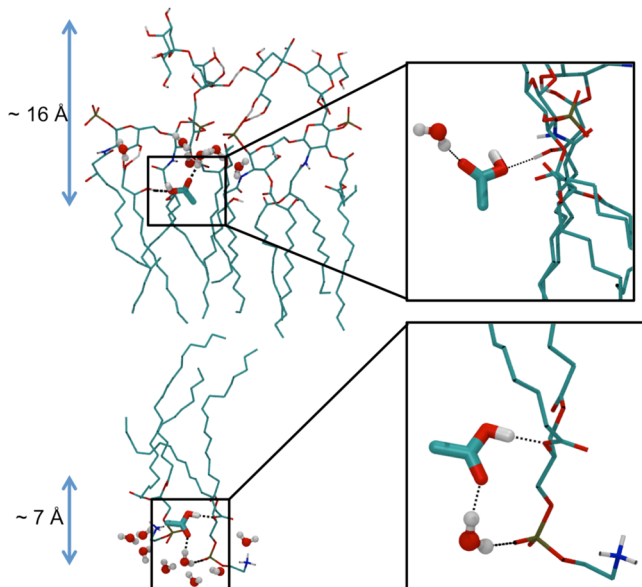


Figure 5. Interactions of acetic acid with water and lipid molecules. Interaction with phospholipids is shown in the bottom half of the figure, and interaction with LPS is shown in the top half of the figure. The widths of the two headgroup regions are indicated by the arrows on the left-hand side.

The hydrophobic core of the membrane provides an energetically unfavorable environment for both polar solutes, with a maximum free energy of $\sim 4.8 \text{ kcal mol}^{-1}$. In contrast, permeation across the LPS headgroup region is energetically favorable. Permeation of these solutes into the membrane core is accompanied by water entry into this region, from both leaflets of the membrane. These solutes are “solvated” by 3–5 water molecules in the hydrophobic region of the bilayer, which stabilize the solutes through hydrogen bonding interactions (Figure 6). Water molecules entered the bilayer from both leaflets and remained within the hydrophobic region for up to $\sim 10 \text{ ns}$. Similar permeation of water into the core of the membrane is not observed for the hydrophobic solutes. We note that the protonation state of acetic acid is likely to differ when in bulk water, compared to the membrane regions as described by MacCallum et al.⁹ In these simulations we have sampled only a single protonation state; acetic acid is protonated in all of the umbrella sampling windows.

A key difference between the physical properties of the two leaflets of the outer membrane is that the lipids diffuse an order of magnitude faster in the inner leaflet, compared to the outer,

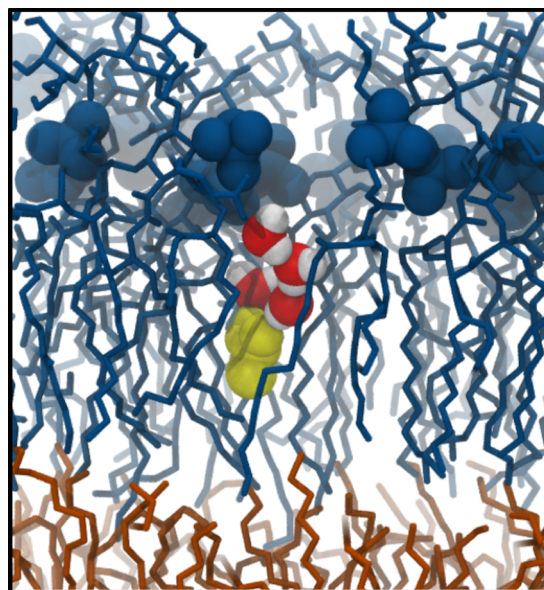


Figure 6. Four water molecules solvating acetic acid within the hydrophobic region of the outer membrane. The solute experiences an energetic barrier in this region.

LPS-containing leaflet. Thus, it is instructive to evaluate the relative diffusion rates of the solutes of interest in this study, in both leaflets. Diffusion of the solutes is generally faster in the membrane core compared to both headgroup regions. The diffusion is also approximately twice as fast through the inner leaflet than the outer leaflet (Figure 7), which is to be expected given their differing compositions.

Diffusion is slowest in the lipid A headgroup regions. Thus, our results suggest that hydrophobic solutes are likely to accumulate in the outer leaflet; there is an energetic barrier to entry, and once they do enter, they diffuse slowly. While the overall trend in the diffusion profiles is similar to the hydrophobic solutes, with diffusion fastest in the membrane core and slowest in the LPS headgroup region, there is a marked difference in the rates of diffusion of the polar solutes in the various regions of the simulated systems. The plot in Figure 7 shows a pronounced peak in the diffusion rates for both polar solutes corresponding to the core of the membrane. This is also likely to be a consequence of the smaller cross-sectional area of these compounds. Our results show that all five solutes diffuse approximately 2–3 times as fast in bulk water compared to the membrane core. This is in good agreement with the diffusion profiles calculated for similar compounds (and several identical ones) through a DPPC bilayer.⁶ Furthermore, we also find that the diffusion through the inner leaflet (composed of phospholipids) of our OM model is consistent with diffusion values calculated for a homogeneous DOPC bilayer (see the Supporting Information).

The accuracy of umbrella sampling calculations relies upon convergence and sampling of simulations. Given the chemical complexity of the systems simulated here, it is important to evaluate the convergence of data to ensure the slow lipid motions are captured at each umbrella sampling window. Sampling along the reaction coordinate was evaluated by inspecting the overlap of the histograms that are used in the generation of the PMF curves. For all five solutes excellent overlap of histograms was achieved (the histograms for all solutes are provided in the Supporting Information).

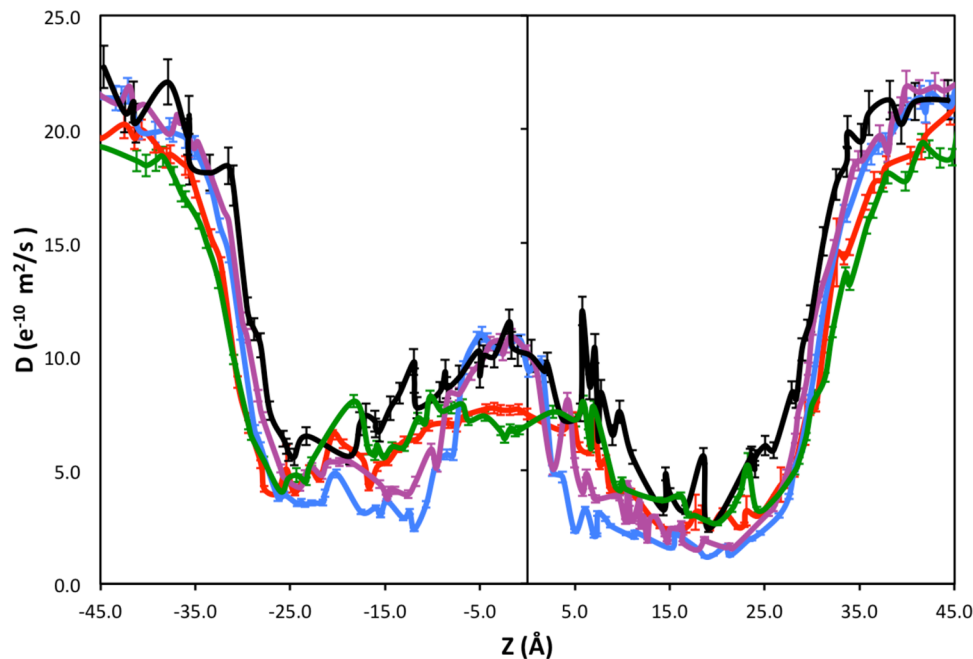


Figure 7. Diffusion of the five solutes as a function of their location in the membrane. Colors are as in Figure 1.

Convergence was evaluated by time-block analysis of the PMF profiles. Time-block analysis for benzene reveals that convergence is achieved after 100 ns.

One of the main challenges in understanding how molecules penetrate directly through the outer membrane of Gram-negative bacteria is in considering the asymmetry of the membrane. Here we show that the chemical differences in the constituents of the two leaflets of the membrane have a profound effect on their permeability, by quantifying the free energy and diffusion profiles through both leaflets. Our results indicate that the free energy change in transferring benzene from water to the LPS headgroup–tail interface is more favorable than for transferring benzene to the headgroup tail region of phospholipids. This is particularly interesting in the context of the outer membrane benzene channel TodX, which has a lateral gate hypothesized to release benzene into the outer leaflet of the outer membrane. Further studies of the protein would be illuminating to investigate if the lateral gate is located at the LPS headgroup–tail interface. It is worth reflecting here on the wider implications of our results; the differing chemical compositions of the two leaflets of the membrane studied here result in asymmetric potential of mean force and diffusion profiles. Given the chemical diversity of biological membranes, this is a significant finding that highlights the need to use appropriate membrane models lest one lose the accuracy gained by the careful setup and performance of time-consuming free-energy calculations by using a biologically irrelevant membrane model! For example, one would expect Gram-positive bacteria such as *Staphylococcus aureus*, which is rich in cationic lysyl-phosphatidylglycerol lipids, to have rather different membrane interactions with small molecules compared to the phosphate-rich outer membranes of Gram-negative bacteria. We have shown that these chemical differences are important.

In summary, our results provide a quantitative measure of the free energy of permeation across the outer membrane of benzene, hexane, ethane, acetic acid, and ethanol, all of which contain functional groups commonly present in antibiotics.

COMPUTATIONAL METHODS

Simulation Protocols. All MD simulations were performed using Gromacs versions 4.5.11 or later and the GROMOS 53a6 force field¹⁰ and SPC3 water model.¹¹ The force field parameters for the lipid molecules are the same as those defined in the work of Piggot et al.¹ The temperature of the system was kept at 310 K using the Nosé–Hoover thermostat with a time constant of 0.5 ps.^{12,13} The pressure of the system was maintained at 1 bar using semi-isotropic pressure coupling implemented with the Parrinello–Rahman barostat with a time constant of 5 ps.¹⁴ Electrostatic interactions were treated using the smooth particle mesh Ewald algorithm, with a short-range cutoff of 1.0 nm.¹⁵ The van der Waals interactions were treated with a 1.0 nm cutoff and a long-range dispersion correction applied to the energy and pressure.

Simulation Setup. Umbrella sampling MD simulations were performed to generate inputs for the calculation of the potentials of mean force (PMFs) along a reaction coordinate perpendicular to the bilayer normal (z -axis) for 6 solutes: ethane, hexane, cyclohexane, benzene, ethanol, and acetic acid for system compositions. The PMFs were calculated using the g_wham implementation of the weighted histogram analysis method (WHAM) within Gromacs. For each substrate, 100 independent simulations were performed (windows) in which the starting configuration of each substrate was separated by 1 Å along the reaction coordinate. The center of mass of the solute was then restrained in the vector of the reaction coordinate using a harmonic force constant of 1000 kJ mol⁻¹ nm². The minimum of the harmonic potential for each window was kept at a constant distance, along the reaction coordinate, based on a reference point in the center of the membrane. The PMF windows spanned the 100 Å system box from $z = -50.0$ to 50.0 Å (z box = 0.0–100.0 Å), with $z = 0$ nm positioned in the bilayer core. The position and force outputs were generated every 2 ps. In the case of insufficient sampling along the reaction coordinate, extra windows were performed at the missing coordinates until the histograms overlapped.

Potentials of Mean Force. The potentials of mean force were calculated using ~100 windows per solute: ethane (~200 windows due to extended sampling in the headgroup regions), hexane, benzene, ethanol (~200 windows, two permeation pathways, with 100 windows each at different lateral starting coordinates), and acetic acid. Addition windows were performed in cases of insufficient sampling. The simulation for each window was run for at least 200 ns. In the generation of the PMFs, the first 10 ns of simulation of data was discarded for equilibration. In the case of the ethane simulations, the first 50 ns was discarded. Additional details of the membrane model, simulation system, and error analyses are provided in the Supporting Information.

Diffusion Calculation. The diffusion coefficients were calculated using an updated methodology as described in Carpenter et al.,¹⁶ based upon the theory of Hummer et al.¹⁷ For each umbrella sampling simulation, the positional variance and autocovariance (at lags from one interval up to 500 intervals) of the compound were calculated. The resulting autocovariance curve decays roughly exponentially with increasing lag time. The characteristic time of the autocovariance decay ("τ") was estimated by making a least-squares fit to the log of the autocovariance data. The diffusion coefficient was then calculated as

$$D(\langle Z \rangle) = \frac{\text{var}(Z)}{\tau_Z}$$

where $\langle Z \rangle$ is the average z-axis position of the compound's center of mass and $\text{var}(z)$ is the variance of the compound's center of mass (the autocovariance at "lag zero").

■ ASSOCIATED CONTENT

● Supporting Information

The Supporting Information is available free of charge on the ACS Publications website at DOI: [10.1021/acs.jpclett.6b01399](https://doi.org/10.1021/acs.jpclett.6b01399).

Details of the membrane model, radial distribution functions of benzene and hexane in the phospholipid headgroup region, diffusion profiles of ethanol in symmetric and asymmetric membrane models, and bootstrapping and histogram overlap analysis for all five solvents ([PDF](#))

■ AUTHOR INFORMATION

Corresponding Author

*E-mail: S.Khalid@soton.ac.uk.

Notes

The authors declare no competing financial interest.

■ ACKNOWLEDGMENTS

We acknowledge use of the Iridis III and IV supercomputers at the University of Southampton. We also thank Livermore Computing for the computing time. Part of this work was performed under the auspices of the U.S. Department of Energy by Lawrence Livermore National Laboratory under Contract DE-AC52-07NA27344, LLNL-JRNL-685118.

■ REFERENCES

- (1) Piggot, T. J.; Holdbrook, D. A.; Khalid, S. Electroporation of the *E. coli* and *S. Aureus* Membranes: Molecular Dynamics Simulations of Complex Bacterial Membranes. *J. Phys. Chem. B* **2011**, *115*, 13381–13388.

- (2) Breidenstein, E. B.; de la Fuente-Nunez, C.; Hancock, R. E. *Pseudomonas Aeruginosa: All Roads Lead to Resistance*. *Trends Microbiol.* **2011**, *19*, 419–426.

- (3) Bemporad, D.; Luttmann, C.; Essex, J. W. Computer Simulation of Small Molecule Permeation Across a Lipid Bilayer: Dependence on Bilayer Properties and Solute Volume, Size, and Cross-sectional area. *Biophys. J.* **2004**, *87*, 1–13.

- (4) Wennberg, C. L.; van der Spoel, D.; Hub, J. S. Large Influence of Cholesterol On Solute Partitioning into Lipid Membranes. *J. Am. Chem. Soc.* **2012**, *134*, 5351–5361.

- (5) Kumar, S.; Bouzida, D.; Swendsen, R. H.; Kollman, P. A.; Rosenberg, J. M. The weighted histogram analysis method for free-energy calculations on biomolecules. *J. Comput. Chem.* **1992**, *13*, 1011–1021.

- (6) Bemporad, D.; Luttmann, C.; Essex, J. W. Behaviour of Small Solutes and Large Drugs in a Lipid Bilayer from Computer Simulations. *Biochim. Biophys. Acta, Biomembr.* **2005**, *1718*, 1–21.

- (7) Chetwynd, A.; Wee, C. L.; Hall, B. A.; Sansom, M. S. The Energetics of Transmembrane Helix Insertion into a Lipid Bilayer. *Biophys. J.* **2010**, *99*, 2534–2540.

- (8) Abraham, M. H.; Whiting, G. S.; Fuchs, R.; Chambers, E. J. Thermodynamics of Solute Transfer from Water to Hexadecane. *J. Chem. Soc., Perkin Trans. 2* **1990**, *2*, 291–300.

- (9) MacCallum, J. L.; Bennett, W. F.; Tieleman, D. P. Partitioning of Amino Acid Side Chains Into Lipid Bilayers: Results from Computer Simulations and Comparison to Experiment. *J. Gen. Physiol.* **2007**, *129*, 371–377.

- (10) Oostenbrink, C.; Soares, T. A.; van der Vegt, N. F.; van Gunsteren, W. F. Validation of the 53A6 GROMOS Force Field. *Eur. Biophys. J.* **2005**, *34*, 273–284.

- (11) Berweger, C. D.; van Gunsteren, W. F.; Mullerplathe, F. Force-field Parametrization by Weak-coupling - Reengineering SPC water. *Chem. Phys. Lett.* **1995**, *232*, 429–436.

- (12) Nose, S.; Klein, M. L. Constant Pressure Molecular-Dynamics for Molecular-Systems. *Mol. Phys.* **1983**, *50*, 1055–1076.

- (13) Hoover, W. G. Canonical Dynamics: Equilibrium Phase-space Distributions. *Phys. Rev. A: At., Mol., Opt. Phys.* **1985**, *31*, 1695–1697.

- (14) Parrinello, M.; Rahman, A. Polymorphic Transitions in Single-crystals - a New Molecular Dynamics Method. *J. Appl. Phys.* **1981**, *52*, 7182–7190.

- (15) Essmann, U.; Perera, L.; Berkowitz, M. L.; Darden, T.; Lee, H.; Pedersen, L. G. A Smooth Particle Mesh Ewald Method. *J. Chem. Phys.* **1995**, *103*, 8577–8593.

- (16) Carpenter, T. S.; Kirshner, D. A.; Lau, E. Y.; Wong, S. E.; Nilmeier, J. P.; Lightstone, F. C. A Method to Predict Blood-brain Barrier Permeability of Drug-like Compounds Using Molecular Dynamics Simulations. *Biophys. J.* **2014**, *107*, 630–641.

- (17) Hummer, G. Position-dependent Diffusion Coefficients and Free Energies from Bayesian Analysis of Equilibrium and Replica Molecular Dynamics Simulations. *New J. Phys.* **2005**, *7*, 34.